# Three Dimensional Rendering of the Mitochondrial Sheath Morphogenesis During Mouse Spermiogenesis

HAN-CHEN HO[1*] AND SHIUAN WEY[2]
[1]*Department of Anatomy, Institute of Integrative Physiology and Clinical Sciences, Tzu Chi University, Hualien, Taiwan*
[2]*Department of Life Science, National Taiwan University, Taipei, Taiwan*

*KEY WORDS* spermatogenesis; 3D reconstruction; electron microscopy

*ABSTRACT* In the middle piece of mouse sperm tail, the idea of the mitochondria wrapping in a sinistral (left-handed) double helical structure was generally accepted. In the existing model, mitochondria aligned in four longitudinal rows (stage 1) and twisted dextrally (right-handed) (stage 2) and began to stagger, where opposing rows of mitochondria contacted each other to form a sinistral double helix (stage 3), finally, the end-on touching mitochondria further elongated to their mature length (stage 4). However, in this model, mitochondria need to shift a long distance and reposition themselves. Since no gaps have been found in mitochondrial sheath, repositioning of most mitochondria along the middle piece is unlikely to happen. Therefore, we reapproached the questions through three-dimensional rendering to provide a new model for mitochondrial sheath formation. In our proposed model, four dextrally arranged spherical mitochondrial arrays were considered stage 1 (resembles stage 2 of the old model). In stage 2 (resembles stage 3 of the old model), a critical difference was found that pairs of mitochondria from the opposing arrays formed ring-like structures instead of a sinistral double helix. In stage 3, which was not observed in the old model, mitochondria staggered in a specific pattern to form the sinistral double helix. In stage 4, mitochondria elongated from crescent-shaped to rod-shaped structures. The new model proposed here would allow each mitochondrion to stay at where they attached first and elongate laterally from two directions to reach their final double helical structure without unreasonable great distance shift along the outer dense fibers. *Microsc. Res. Tech. 70:719–723, 2007.* 

## INTRODUCTION

The middle piece of mammalian sperm is characterized by a mitochondrial helical sheath that surrounds the axonemal complex and the nine outer dense fibers (Fawcett, 1975). The remarkable regularity in the organization of mitochondrial sheath was found in several mammalian species, such as the little brown bat (Fawcett and Ito, 1965), the woolly opossum (Phillips, 1970), and the Chinese hamster (Phillips, 1977). It is intriguing that the length of the middle piece and the number of gyres of the mitochondrial sheath are uniform and heritable within the same mammalian species (Woolley and Beatty, 1967). However, the mechanisms regulating the regular spatial distribution and synchronized development of the helical mitochondrial arrays are not completely understood. A precisely regulated mitochondrial sheath formation is critical for sperm motility and fertility. Male knockout mice such as *Gopc*$^{-/-}$ and *Nectin-2*$^{-/-}$ are infertile partly due to defects in mitochondrial helical sheath development during spermiogenesis (Bouchard et al., 2000; Suzuki-Toyota et al., 2004).

Development of the mitochondrial helical sheath was studied by using several different methods since the 1970s; however, surface replication (Woolley, 1970), conventional scanning electron microscopy (SEM) (Baradi and Rao, 1979), or cryo-fracturing method with high resolution SEM (Otani et al., 1988) were not satisfactory for observing mitochondrial sheath development at 360°. Although Otani et al. (1988) presented four synchronized developmental stages describing mitochondrial sheath formation during spermiogenesis, more questions were brought up. According to their model, mitochondria were arranged in four longitudinal rows in stage 1; twisted dextrally and began to stagger in stage 2; formed a sinistral double helix by contacting the opposing rows of mitochondria in stage 3; elongated to their final mature length and shape in stage 4. However, elongation of end-to-end touching mitochondria from one half of 1 gyre (stage 3) to three-fifth of 1 gyre (stage 4) would lead to a "spinning effect"—each mitochondrion would push the next contacting mitochondrion and result in spinning of mitochondria along the outer dense fibers. In their model, most mitochondria need to shift a long distance from where they originally attached, and reposition themselves because the diameter of each mitochondrion decreased about 50% in the elongation process. Considering the repositioning of most mitochondria along the

This article contains supplementary material available via the Internet at http://www.interscience.wiley.com/jpages/1059-910X /suppmat.

*Correspondence to: Han-Chen Ho, 701, Sec. 3, Chung-Yang Rd., Hualien 97004, Taiwan. E-mail: hcho@mail.tcu.edu.tw

Present address of Shiuan Wey: Programs in Biomedical & Biological Sciences, University of Southern California, Los Angeles, CA 90089, USA.

Received 26 October 2006; accepted in revised form 1 February 2007

Contract grant sponsor: National Science Council, Taiwan, Republic of China; Contract grant numbers: 94-2320-B-320-010, 95-2311-B-320-004.

DOI 10.1002/jemt.20457

Published online 24 April 2007 in Wiley InterScience (www.interscience.wiley.com).

middle piece and no gaps have been found in mitochondrial sheath, this is unlikely to happen. Therefore, we revisited the questions and took advantage of the new image processing software to reconstruct mature mouse sperm middle piece from ultrathin serial sections. For the first time, we are able to look at the mitochondrial helical sheath from any angle of view.

## MATERIALS AND METHODS

### Animals and Tissue Collection

Mature male ICR mice were sacrificed by $CO_2$ inhalation and cervical dislocation. Testes and epididymides were removed and prepared as follows for ultrastructural observations. The experimental protocol was approved by the Institutional Animal Care and Use Committee of Tzu Chi University.

### Scanning Electron Microscopy

Tissue blocks of testes were prepared by cryo-fracturing method according to Tanaka (1989) with some modifications (Ho et al., 1999). Specimens were fixed with 1% osmium tetroxide ($OsO_4$) in 0.1 M cacodylate buffer (pH 7.2) at 0–4°C for 1 h, rinsed with cacodylate buffer, and then immersed in 25 and 50% DMSO for cryoprotection. The specimens were frozen in liquid propane and cracked into small pieces in liquid nitrogen. Tissue fragments were thawed in 50% DMSO and post-fixed with 1% $OsO_4$ in cacodylate buffer, and then immersed in 0.1% $OsO_4$ at 20°C for 18 h. The specimens were dehydrated through a graded series of ethanol solution and critical point dried with a Hitachi HCP-2 critical point dryer (Hitachi, Tokyo, Japan). After being coated with gold, the specimens were examined with a Hitachi S-800 or S-4700 field emission scanning electron microscope (Hitachi).

### Transmission Electron Microscopy

Small blocks of testes and cauda epididymides were prefixed with 2.5% glutaraldehyde/0.1 M cacodylate buffer containing 2% tannic acid at 0–4°C for 1 h, and post-fixed with 1% $OsO_4$/0.1 M cacodylate buffer for 1 h at room temperature. After fixation, specimens were dehydrated through a graded series of ethanol and then embedded in Spurr's resin. Serial ultrathin sections around 80 nm were made with a Leica Ultracut R ultramicrotome (Leica, Heerbrugg, Switzerland) and examined with a Hitachi H-7500 transmission electron microscope at 80 kV after staining with uranyl acetate and lead citrate.

### Three-Dimensional (3D) Reconstruction

Magnification was calibrated using diffraction grating replica (2160 lines/mm, Ted Pella, Inc., Redding, CA). Section thickness averaged at 80 nm was used for reconstruction. Images taken from each set of serial sections were used to reconstruct its 3D image with the software *Reconstruct* (www.synapses.bu.edu). Serial images were aligned by identifying several pairs of corresponding points in adjacent sections, using a least-squares linear fit (Fiala, 2005; Fiala and Harris, 2001). Relevant structures of the mitochondria were traced with a "closed point-by-point drawing" tool (available in the "Tools" box of the software) at a zoomed view under higher magnification. The 3D scene was rendered using OpenGL (www.opengl.org). Then it was exported as a 3D model as a Visual Reality Modeling Language (VRML) file. The VRML files were played and recorded as video files for viewing.

Fig. 1. Synchronized development of mouse spermatids in a given cryo-fractured surface. Three spermatids at step 15 show the early stage of mitochondrial sheath formation. At the middle pieces where plasma membranes were removed, spherical mitochondria are regularly aligned in a dextral array fashion. Bar = 5 μm.

## RESULTS

In the mouse, formation of the mitochondrial helical sheath was observed to begin at late spermiogenesis around step 15 (Russell et al., 1990). Mouse seminiferous tubules showed certain patterns of cellular association (stage) in a cyclic process (wave) (Russell et al., 1990). Therefore, on any given cryo-fractured surface of the seminiferous tubule, spermatids with mitochondria at the same stage of development were easily observed (Fig. 1). The developmental process can be divided into four stages according to our findings. At stage 1, spherical mitochondria lined up regularly around the outer dense fibers of the middle piece, forming four dextral longitudinal arrays (Figs. 1 and 2A). The adjacent two arrays of spherical mitochondria were alternately arranged (Fig. 2A). At stage 2, all spherical mitochondria became crescent shaped, and the elongating two ends staggered between the mitochondria at the adjacent arrays (Fig. 2B). On a fracturing surface where some mitochondria were lost during sample preparation, the elongating two ends of those crescent-shaped mitochondria were clearly seen attached on and proceeded laterally along the outer dense fibers (Fig. 2C). This first staggering process transformed the four dextral helical arrays into about

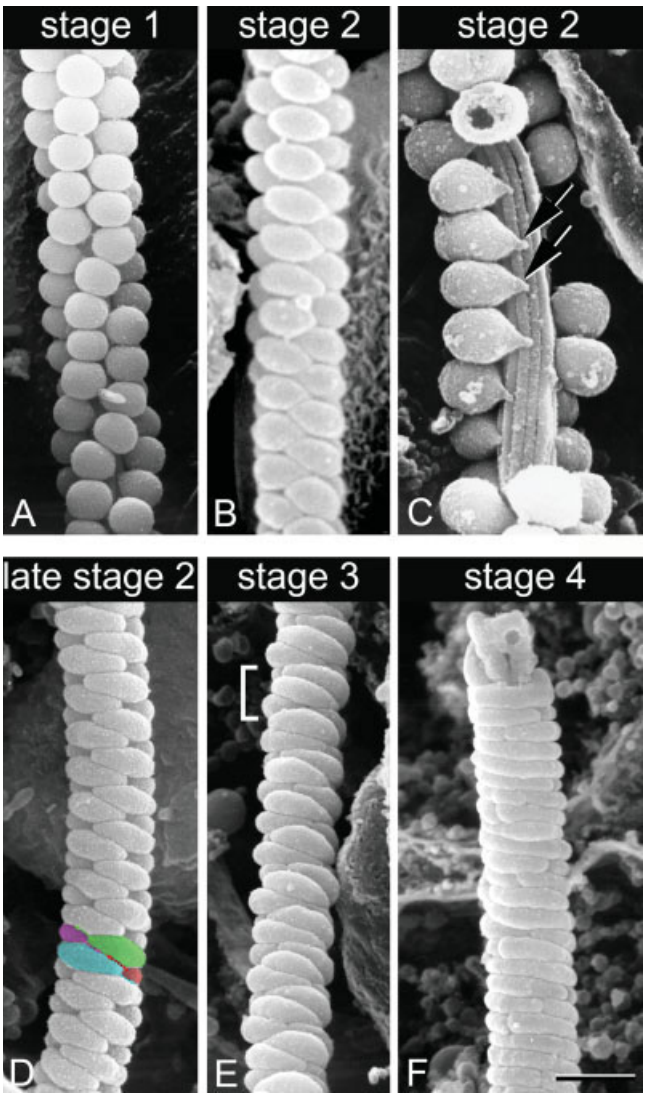


Fig. 2. Mitochondrial helical sheath development. (**A**) Stage 1: During step 15 of mouse spermiogenesis, mitochondria lined up regularly and attached on the outer dense fibers around middle piece, forming four dextral helical arrays. Mitochondria at this stage are spherical. (**B**, **C**) Stage 2: Mitochondria elongated laterally (arrows) and became crescent-shaped. (**D**) In late stage 2, pairs of mitochondria from the opposing arrays contacted each other forming a doughnut-shaped structure. Arrows and pseudocolors indicate future mitochondrial staggering directions in stage 3. Note after the second staggering process, the depicted magenta and red mitochondria will contact each other as shown in Figure 4D. (**E**) Stage 3: Mitochondria continued to elongate and stagger in a specific pattern as shown in D and Figure 4, which transformed the mitochondrial sheath into a double helical structure. At the end of stage 3, special segmented repeating pattern (parenthesis) is obvious. (**F**) Stage 4: Crescent-shaped mitochondria elongated to three-fifth of 1 gyre and became rod-shaped. Bar = 1 μm (A, B, D–F) and 0.8 μm (C).

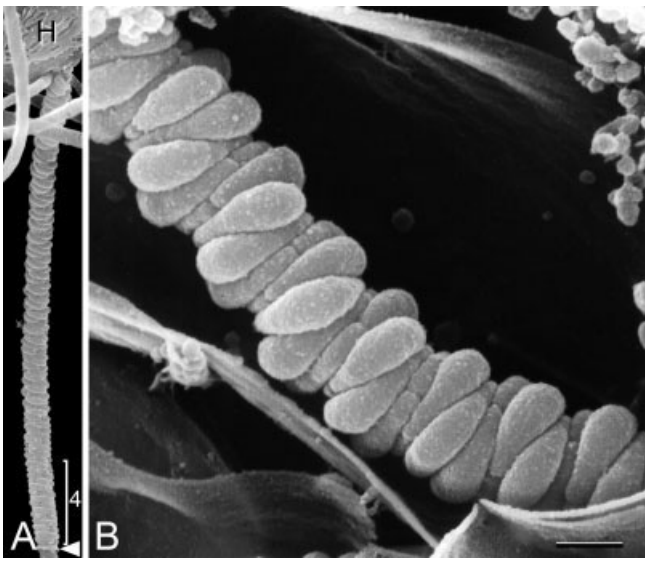


Fig. 3. A special segmented repeating pattern is characteristic of stage 3 mitochondrial sheath. (**A**) A late spermatid showing the whole middle piece where the proximal part is in stage 3 and the distal part is in stage 4 (]4). H, spermatid head; arrowhead: annulus. (**B**) A higher magnification on the special segmented repeating pattern found in stage 3. Bar = 0.5 μm (A) and 2.5 μm (B).

70 doughnut-like structures by connecting each pair of the mitochondria in opposing two arrays into one ring-like structure. At the end of stage 2, crescent-shaped mitochondria each spanned one half of 1 gyre (Fig. 2D). At stage 3, mitochondria continued to elongate to three-fifth of 1 gyre and made their second staggering process, which transformed the mitochondrial sheath into a special and regular pattern that has not been discovered before (Figs. 2E and 3). From a closer look on the middle piece, transformation of the mitochondrial sheath into the next stage always starts from the distal end (right above the annulus) of the middle piece (Fig. 3), which made staging easier. During this second staggering process, mitochondria slide past each other at the contact point in a specific pattern: if looking towards the contact point of two mitochondria, the mitochondrion on the left-hand side staggered distally to the contact point, while the mitochondrion on the right-hand side staggered proximally to the contact point, making a final sinistral double helical strucuture (Figs. 2D, 2E, 3B, 4C, and 4D). At stage 4, the crescent-shaped mitochondria became rod-shaped and abutted end to end. Each mitochondrion spanned three-fifth of 1 gyre, and the mitochondrial sheath remained a sinistral double helix (Fig. 2F) as found in mature sperm.

Although the cryo-fracturing method combined with the SEM revealed much more 3D information on mitochondrial sheath development, it did not allow us to observe each single mouse sperm tail from the whole 360°. To solve this problem, we reconstructed mouse sperm middle pieces from serial ultrathin sections to elucidate the 3D transformation of mitochondrial helical sheath in more detail (Fig. 4 and Movies S1–S3 in the Supplemental Data). For the first time, the sinistral double helical structure is unequivocally revealed (Fig. 5 and Movie S4 in the Supplemental Data). The 3D result further supported our findings described earlier.

## DISCUSSION

In this study, we reconstructed the 3D structure of the mouse sperm middle piece from serial ultrathin sections to reveal the real spatial configuration of the

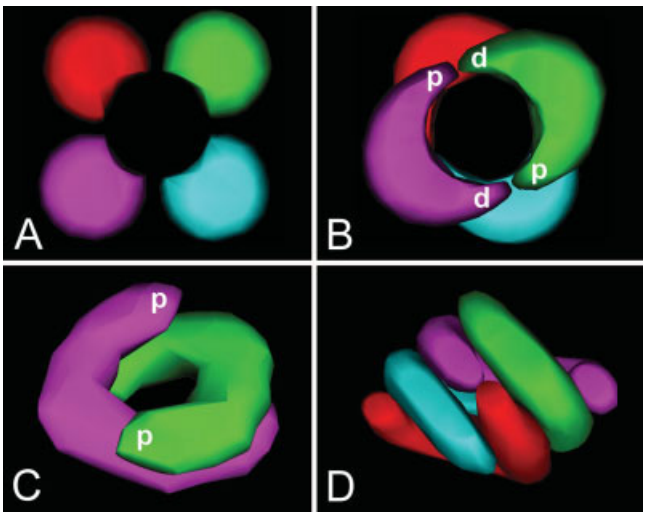


Fig. 4. Still images of 3D reconstructed models showing representative mitochondria at stages 1–3. (**A**) Four spherical mitochondria surrounding the axoneme and outer dense fibers (the central empty space) are found at stage 1. (**B**) Mitochondria at the opposing arrays (e.g. green- and magenta-colored mitochondria) form a doughnut-shaped structure at stage 2. (**C**) At stage 3, each pair of doughnut-shaped mitochondria found in stage 2 slide past each other in a specific pattern, where one end moves distally (d), and the other moves proximally (p) as shown here. (**D**) The second staggering process transformed the mitochondrial sheath into a double helical structure, in this case, one strand contains green- and cyan-colored mitochondria, the other one contains magenta- and red-colored mitochondria. Different colors of mitochondria are used for presentation purpose only. Still images A–C represent structures found when looking in a proximal to distal direction. The 3D animated scene of each stage is provided in the Supplemental Data.

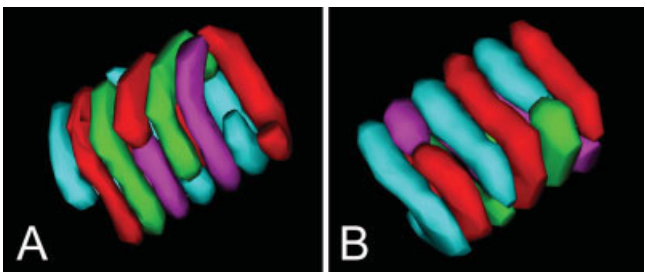


Fig. 5. Still images of 3D reconstructed mitochondrial sheath at stage 4. (**A**) One segment of reconstructed mature mitochondrial sheath showing 10 mitochondria wrapping in a double helical fashion: the red- and magenta-colored mitochondria form one strand, and the green- and cyan-colored mitochondria form the other strand. (**B**) Still image of the same reconstructed mitochondrial sheath shown in (A) but turned 180° along the longitudinal axis of the sperm tail. The 3D animated scene is provided in the Supplemental Data.

sperm tail during mitochondrial sheath formation. For the first time, a 360° view of the developing and final mitochondrial helical sheath can be easily appreciated.

Early in the 1970s, Woolley (1970) proposed that the mitochondrial sheath of mouse sperm wraps in a double helical structure using surface replication. Later on, Otani et al. (1988) presented better 3D images of mitochondrial sheath using cryo-fracturing method and SEM, and concluded a sinistral double helical structure in the middle piece. However, Otani et al. proposed that after forming a double helical structure, mitochondria elongate from one half of 1 gyre to three-fifth of 1 gyre to complete the mitochondrial sheath formation. Considering the end-to-end touching configuration of mitochondria, the final elongation process proposed by Otani et al. would have caused pushing and spinning of the connecting mitochondria either proximally or distally to accommodate the longer mitochondria. In addition to the spinning effect, most mitochondria would also need to shift a long distance from where they originally attached in order to reposition themselves because the diameter of each mitochondrion decreased about 50% in the elongation process (Otani et al., 1988). However, no gaps have been observed during mitochondrial sheath formation after stage 2. Also, one has to wonder what would provide the motile force for spinning and shifting the mitochondria, if the old model was correct.

In our study, we found a special stage in mitochondrial sheath development (Figs. 2E and 3) that has not been discovered by Otani et al. (1988). We propose that in the first staggering stage, mitochondria formed closed ring-like structure (stage 2) instead of the double helical structure. It is not until the next stage (stage 3) that the mitochondria staggered once again to transform into the double helical structure. The model proposed here would allow each mitochondrion to stay at where they attached on the outer dense fibers in the first place, and elongate laterally from two directions to reach their final double helical structure without unreasonable great distance shift along the outer dense fibers. In addition, the reconstructed 3D images provided a clear picture on how the mitochondrial sheath wrap in the middle piece in mature sperm tail.

The synchronism and regularity in mitochondrial sheath development pose challenging questions concerning the factors that precisely regulate the mitochondrial morphogenesis. Although largely unknown, the cytoskeletal components found between mitochondria and the outer dense fibers were speculated to play a critical role in guiding and anchoring the mitochondria to their precise spatial arrangement in the developing middle piece (Olson and Winfrey, 1986, 1990). Recently, spergen-1, a small protein specifically localized in the mitochondria of rat elongating spermatids and mature sperm, was found to mediate mitochondrial aggregation, and was speculated to function as an adhesive molecule to assemble mitochondria into the mitochondrial sheath around the middle piece during spermiogenesis (Doiguchi et al., 2002). To find out more about the molecular basis of mitochondrial sheath formation, understanding the structural basis of mitochondrial sheath formation may provide insights into the potential factors and mechanisms. In addition, it might shed light on some cases of male infertility resulting from flagellar defects (Olson et al., 2004). In gossypol-treated animals, both a mitochondrial sheath truncation and an assortment of mitochondrial defects have been reported in spermatids and epididymal spermatozoa (Chenoweth et al., 2000; Oko and Hrudka, 1982). Infertile male knockout mice such as *Gopc*$^{-/-}$ and *Nectin-2*$^{-/-}$ also showed defects in mitochondrial sheath development during spermiogenesis (Bouchard et al., 2000, Suzuki-Toyota et al., 2004). These reported sperm middle piece abnormalities may have a common underlying mechanistic origin, and it would be interesting

to investigate it through both molecular and ultrastructural approaches.

Although time consuming, reconstructing 3D structures from serial ultrathin sections revealed much more additional information and enhanced our understanding on cellular ultrastructures. This technique can be used in conjunction with traditional TEM, having advantages on higher resolution without losing the spatial details.

## REFERENCES


Baradi AF, Rao NS. 1979. On the development of midpiece mitochondria of mouse spermatozoa. Cell Tissue Res 199:349–352.

Bouchard MJ, Dong Y, McDermott BM Jr, Lam DH, Brown KR, Shelanski M, Bellve AR, Racaniello VR. 2000. Defects in nuclear and cytoskeletal morphology and mitochondrial localization in spermatozoa of mice lacking nectin-2, a component of cell-cell adherens junctions. Mol Cell Biol 20:2865–2873.

Chenoweth PJ, Chase CC, Risco CA, Larsen RE. 2000. Characterization of gossypol-induced sperm abnormalities in bulls. Theriogenology 53:1193–1203.

Doiguchi M, Mori T, Toshimori K, Shibata Y, Iida H. 2002. Spergen-1 might be an adhesive molecule associated with mitochondria in the middle piece of spermatozoa. Dev Biol 252:127–137.

Fawcett DW. 1975. The mammalian spermatozoon. Dev Biol 44:394–436.

Fawcett DW, Ito S. 1965. The fine structure of bat spermatozoa. Am J Anat 116:567–609.

Fiala JC. 2005. Reconstruct: A free editor for serial section microscopy. J Microsc 218:52–61.

Fiala JC, Harris KM. 2001. Cylindrical diameters method for calibrating section thickness in serial electron microscopy. J Microsc 202:468–472.

Ho HC, Tang CY, Suarez SS. 1999. Three-dimensional structure of the Golgi apparatus in mouse spermatids: A scanning electron microscopic study. Anat Rec 256:189–194.

Oko R, Hrudka F. 1982. Segmental aplasia of the mitochondrial sheath and sequelae induced by gossypol in rat spermatozoa. Biol Reprod 26:183–195.

Olson GE, Winfrey VP. 1986. Identification of a cytoskeletal network adherent to the mitochondria of mammalian spermatozoa. J Ultrastruct Mol Struct Res 94:131–139.

Olson GE, Winfrey VP. 1990. Mitochondria-cytoskeleton interactions in the sperm midpiece. J Struct Biol 103:13–22.

Olson GE, Winfrey VP, Hill KE, Burk RF. 2004. Sequential development of flagellar defects in spermatids and epididymal spermatozoa of selenium-deficient rats. Reproduction 127:335–342.

Otani H, Tanaka O, Kasai K, Yoshioka T. 1988. Development of mitochondrial helical sheath in the middle piece of the mouse spermatid tail: Regular dispositions and synchronized changes. Anat Rec 222:26–33.

Phillips DM. 1970. Ultrastructure of spermatozoa of the wooly opossum Caluromys philander. J Ultrastruct Res 33:381–397.

Phillips DM. 1977. Mitochondrial disposition in mammalian spermatozoa. J Ultrastruct Res 58:144–154.

Russell LD, Ettlin RA, Sinha Hikim AP, Clegg ED. 1990. Histological and histopathological evaluation of the testis. Clearwater: Cache River Press. p. 286

Suzuki-Toyota F, Ito C, Toyama Y, Maekawa M, Yao R, Noda T, Toshimori K. 2004. The coiled tail of the round-headed spermatozoa appears during epididymal passage in GOPC-deficient mice. Arch Histol Cytol 67:361–371.

Tanaka K. 1989. High resolution scanning electron microscopy of the cell. Biol Cell 65:89–98.

Woolley DM. 1970. The midpiece of the mouse spermatozoon: Its form and development as seen by surface replication. J Cell Sci 6:865–879.

Woolley DM, Beatty RA. 1967. Inheritance of midpiece length in mouse spermatozoa. Nature 215:94–95.